Nonthermal Electron Velocity Distribution Measured by Electron Cyclotron Emission in Alcator C Tokamak

K. Kato and I. H. Hutchinson

Plasma Fusion Center, Massachusetts Institute of Technology, Cambridge, Massachusetts 02139

(Received 4 November 1985)

The nonthermal electron velocity distribution of lower-hybrid-rf–heated plasmas in the Alcator C tokamak is deduced from measurements of electron-cyclotron emission with a specialized vertical-viewing optics arrangement. At a density of $\bar{n}_e = 0.7 \times 10^{20}$ m^{-3}, the reconstructed distribution function in the range 50 keV $\leq E \leq$ 230 keV shows enhancement in the parallel direction with a perpendicular spread equivalent to $T_\perp \approx 30$ keV. The line-average energetic electron density in this energy range is approximately 10^{17} m^{-3} during the rf.

PACS numbers: 52.25.Sw, 52.55.Fa

In this Letter we report on the nonthermal electron-velocity distribution obtained from the vertical-viewing electron-cyclotron emission (ECE) diagnostic on Alcator C ($R = 64$ cm, $a = 16.5$ cm, $B_T = 8$ T). In the past, ECE measurements of the distribution were limited to a fit of a few parameters (e.g., $T_\perp$ and $T_\parallel$); some of these measurements are reviewed by Boyd.[1] In comparison, by use of our configuration, rather general distributions can be diagnosed in significant detail with a minimum of assumptions about their shape. Recent experiments using first harmonic absorption in vertical propagation have been performed on the Princeton Large Torus.[2]

The theoretical principles of the present method are discussed in detail elsewhere,[3] but we summarize them here. When perpendicular electron-cyclotron emission from a region of approximately constant magnetic field is observed, the frequency shift is entirely due to the relativistic mass-increase factor, γ: $\omega = l\Omega/\gamma$, where l is the cyclotron harmonic number, and Ω is the fundamental rest-mass cyclotron frequency. In this specialized situation, it is possible to discriminate among electrons according to their total energy, provided overlap of the neighboring harmonics does not occur.

The ECE intensity in this case yields information regarding the distribution of electrons in momentum space. Under the assumption of negligible absorption, the observed intensity is proportional to the emissivity, which can be written as an integral of $f(\mathbf{p})$ over the momentum pitch angle, weighted by the single-particle emissivity and corrected for finite plasma effects.[4] (The momentum is in natural units: $p = \gamma v/c$.) The unnormalized electron distribution function, $f(\mathbf{p})$, is expressed as

$$f(\mathbf{p}) = f_p(p) f_\theta(p, \theta), \tag{1}$$

where $f_p(p)$ is the mean phase-space density of electrons at p, and we choose

$$f_\theta(p, \theta) = L \exp\{-\Lambda(p)\cos^2\theta\} \tag{2}$$

as the pitch-angle distribution, with a normalization $\int_0^\pi f_\theta(p, \theta)\sin\theta\, d\theta = 2$. This choice of f_θ is appropriate, though not unique. It is a Gaussian-type function along the circular resonance contour in momentum space, $p = \text{const}$. The parameter to be fitted, Λ, determines the anisotropy of the distribution along the contour. A negative Λ implies enhancement in the parallel direction (prolate distribution), while positive Λ implies loss-cone type of anisotropy (oblate). For strong anisotropies ($|\Lambda| \gg 1$), this pitch-angle distribution describes a Gaussian spread in the "narrow" direction. The anisotropy factor Λ can be obtained independently of f_p from ratios of two harmonic intensities of the same electron energy, for example, $I(3\omega)/I(2\omega)$. Then the absolute intensity of a single harmonic yields f_p. Perpendicular emission gives no information on any parallel asymmetry in the distribution. However, our symmetric $f(\mathbf{p})$ may be modified to model asymmetric distributions if necessary.

To isolate a region of constant magnetic field, the Alcator C tokamak plasma is viewed vertically from the top of the machine, through the center of the plasma. The spread of the antenna pattern in the major-radius direction is approximately 3 cm at the plasma center, which translates to a field variation of 5%. In order to remove reflected radiation that could introduce spurious emission from other magnetic fields or propagation angles, a compact microwave viewing dump made of Pyrex[5] was placed at the bottom of the vacuum chamber. This dump is essential, because the spot size of the view is larger than the access port at the bottom. Tests using reproducible thermal ECE show the dump to be effective in removing approximately 90% of the unwanted radiation.[6] ECE measured by this configuration cannot yield any spatial resolution (because of the constant B), and is simply a chord-integrated emissivity.

The extraordinary-mode frequency spectrum is obtained every 15 ms by a rapid-scanning Michelson interferometer and liquid-helium–cooled InSb detector. The choice of extraordinary mode is motivated by its higher emissivity and narrower antenna pattern in our

system (because of diffraction) compared to the ordinary mode. The entire optical train has been calibrated for relative frequency response in the range 100 to 900 GHz by use of a mercury arc lamp.[7] The absolute response is obtained from the second-harmonic thermal emission of a plasma discharge of known electron temperature.

In Fig. 1 we show two ECE spectra, one before the rf pulse, and another, a typical spectrum during lower-hybrid rf heating at a density of $\bar{n}_e = 0.7 \times 10^{20}$ m^{-3}. The rf pulse (400 kW) was sustained for 120 ms, and the ECE intensity increased by a factor of 3 during this time, with no dramatic change in spectral features. The spectrum shown is taken approximately 80 ms into the rf pulse. Intense bursts of emission due to nonthermal instabilities occurred at the beginning of the plasma discharge and immediately after the rf shutoff, but none was observed during the pulse. Data were also taken on lower-hybrid current-drive shots. However, the excessive harmonic overlap due to the higher mean energy of the electron population makes the interpretation more difficult, and a reliable distribution has not yet been obtained from them. Therefore, we do not discuss such plasmas here.

The thermal spectrum (broken line) shows that the dump is quite effective in suppressing the emission from outside the line of sight. The second-harmonic–emission (440 GHz) peak has a width consistent with the antenna pattern. (Spectra of the second-harmonic thermal emission *without* the dump show emission from regions all along a major diameter because of multiple reflections.) The emission below

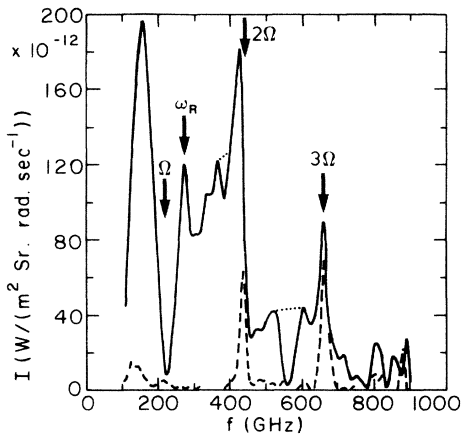

FIG. 1. Extraordinary-mode ECE spectra for nonthermal emission during lower-hybrid rf heating ($\bar{n}_e = 0.7 \times 10^{20}$ m^{-3}, $I_p = 180$ kA, $P_{rf} = 400$ kW, $t = 260$ ms) shown by the solid line, and thermal emission just prior to rf injection of the same discharge ($\bar{n}_e = 1.2 \times 10^{20}$ m^{-3}, $I_p = 270$ kA, $t = 180$ ms, $T_{e0} = 2.5$ keV) shown by the broken line. Deuterium discharge, $B_T = 8$ T, $f_{ce} = 220$ GHz, frequency resolution $\simeq 15$ GHz.

Ω is the "steady" ω_{pe} Cherenkov emission due to the small runaway population present in this discharge.[8]

The nonthermal spectrum (solid line) shows several notable features. The down-shifted first-harmonic emission is seen below Ω (220 GHz). The dip at 220 GHz is due to the bulk-plasma thermal absorption. The narrow peak at 270 GHz we believe to be because the right-hand cutoff layer (ω_R) in the line of sight reflects the antenna pattern away from the dump and hence enhances the intensity observed. The dips at 380 and 560 GHz are atmospheric water-vapor absorption lines, which limit the energy range over which the spectrum can be interpreted quantitatively with full confidence. A dramatic discontinuity is seen just above 2Ω. The substantially lower emission on the high-frequency side is consistent with expectations of purely down-shifted emission and attests to the effectiveness of the dump in suppressing reflected radiation. Overlapping third-harmonic down-shifted radiation continues below the second-harmonic rest-mass frequency, 2Ω, as indicated by the finite intensity just above it. This indicates that some unwrapping of the harmonics is required. Above 3Ω, noise starts to dominate the features because of decreasing response of the detector in this frequency range.

The distribution-function parameters are deduced, as described above, by use of computer code which takes into account the mild harmonic overlap. First, the ratio $I(3\omega)/I(2\omega)$ is used to obtain Λ, and then $I(2\omega)$ is used to obtain f_p in the range $\frac{2}{3}\Omega \leq \omega \leq \Omega$. The harmonic overlap is taken into account by the assumption that the distribution extrapolates to higher energies with approximately the same slope. An iterative procedure is carried out to obtain a set of f_p and Λ that is consistent with the spectrum in the range above the right-hand cutoff peak to 3Ω. Thus the final solution of f_p is consistent with $I(3\omega)$ as well as $I(2\omega)$. For these lower-hybrid rf-heated spectra, the effect of overlap is limited to the low-energy end ($\lesssim 50$ keV) of the distribution for the second harmonic. The first harmonic is excluded from this analysis because of larger uncertainty in the calibration, decreased effectiveness of the dump at low (< 200 GHz) frequencies, and nonnegligible plasma optical depth. The choice of $I(3\omega)/I(2\omega)$ limits the analysis in electron-energy space to below 230 keV.

For the code analysis, the two water lines at 380 and 560 GHz are filled in by linear interpolation between frequencies 364 and 398 GHz, and 519 and 601 GHz (shown by dotted lines in Fig. 1). The actual intensity is at most 15% higher than the interpolated value near 560 GHz and within calibration uncertainty at 380 GHz. These estimates are based on observation of the general shape of the spectra obtained under different conditions, such as different toroidal fields. The resonant electron-energy range unaffected by interpo-

lation is above 140 keV. In view of the previously mentioned right-hand cutoff effect, the region of analysis is terminated before the right-hand cutoff peak at 270 GHz.

The distribution-function parameters, $f_p(p)$ and $\Lambda(p)$, obtained from the spectrum of Fig. 1 are plotted in Fig. 2. Energy is plotted on the abscissa, so that Maxwellian temperature can be obtained by straightforward slope fitting. {No ambiguity arises because of the one-to-one correspondence between E and p, $E = m_0c^2[(p^2+1)^{1/2}-1]$.} Both f_p and Λ are to be interpreted as line-average quantities over the 33-cm chord in the plasma. f_p is decreasing but persistent all the way up to the 230-keV limit. The anisotropy factor Λ is negative and in the range $-6 \leq \Lambda \leq -2$ above 50 keV. At 50 keV, a positive Λ is obtained, probably because of uncertainties in the harmonic-overlap estimate. Since the harmonic ratio is insensitive to Λ for $\Lambda > 0$, we artificially force $\Lambda = 0$ for this energy. A relativistic Maxwellian ($T \approx 80$ keV) may be fitted to f_p as shown by the straight line in Fig. 2(a). This fit will be used to compute absorption coefficients discussed below.

To illustrate the distribution function, contours of constant $f(\mathbf{p})$ are plotted in $(p_\parallel, p_\perp)$ space in Fig. 3. (The 50-keV data are excluded.) This clearly shows the enhancement of the electron population in the parallel direction, as measured by other experiments[9] and predicted by theory.[10] The bump at $p_\parallel \simeq 0.9$ is due to the bump in f_p, although, as the error bars indicate, it is probably not statistically significant.

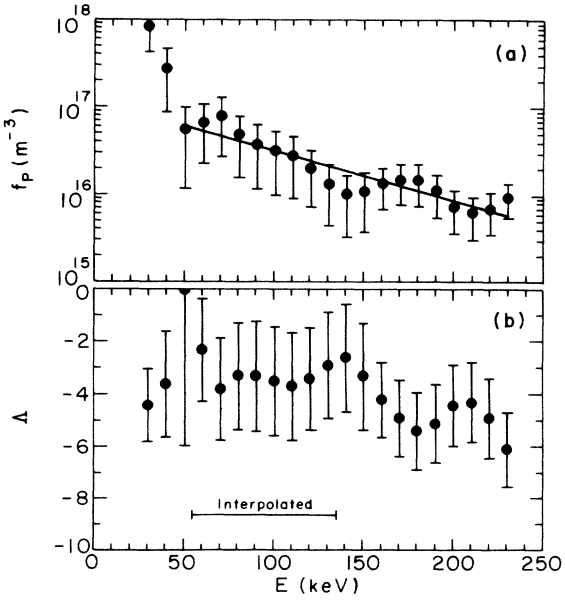

FIG. 2. Distribution function parameters (a) f_p and (b) Λ plotted as functions of the total electron energy. The range of energy for which interpolated data was used is indicated in (b).

The "perpendicular temperature," $T_\perp$, as a function of $p_\parallel$ is also obtainable from $f(\mathbf{p})$. Here it is defined such that the distribution along a $p_\parallel = \text{const}$ cross section best fits the expression

$$f(p_\perp, p_\parallel = \text{const}) = A \exp\left[-\frac{m_0c^2}{T_\perp(p_\parallel)}(1+p_\parallel^2+p_\perp^2)^{1/2}\right]. \quad (3)$$

The perpendicular temperature thus obtained is approximately 30 keV in the range $0.45 \leq p_\parallel \leq 0.95$. Any trend in $T_\perp$ as a function of $p_\parallel$ is difficult to determine because of the large scatter of the data which comes primarily from the bumpiness of f_p.

For comparison, the "perpendicular temperature" is computed from the first-harmonic radiation temperature, T_r, and the absorption coefficient, α. T_r is obtained from the down-shifted first-harmonic intensity ($\omega < \Omega$), and α is calculated from the smoothed f_p shown in Fig. 2(a) and a corresponding smoothed Λ obtained from this f_p and $I(2\omega)$. [This set of smoothed f_p and Λ is only approximately consistent with $I(3\omega)$.] The optical depth, τ, calculated in this way for 50 keV $\leq E \leq$ 230 keV at the second harmonic is $\tau_2 \leq 0.1$, so that the assumption of negligible absorption is justified. In the first harmonic, $\tau_1 \approx 0.4$. Thus, for the observed average radiation temperature $T_r \approx 10$ keV, $T_\perp$ deduced from the first harmonic, $T_\perp \simeq T_r/[1-\exp(-\tau_1)]$, is consistent with that deduced from the second and the third harmonics. The 30-keV perpendicular temperature of the distribution seems reasonable compared with $T_\perp \approx 100$ keV estimated for current-drive plasmas,[9] whose lower-hybrid wave spectrum creates a far more energetic electron tail and therefore higher $T_\perp$ than in the heating case.[11]

A "parallel temperature," $T_\parallel$, of 200 keV is deduced by the fit of a 1D relativistic Maxwellian to the

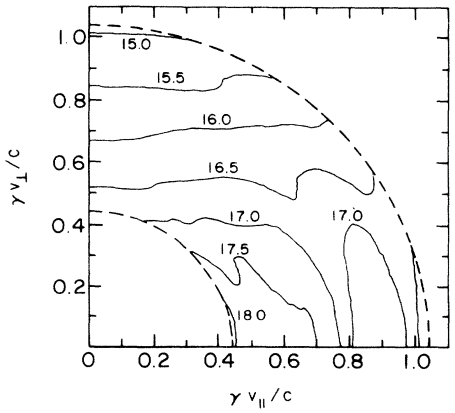

FIG. 3. Distribution-function contour plot for $0.45 \leq p \leq 1.05$ (corresponding to 50 keV $\leq E \leq$ 230 keV); contour magnitudes are given in $\log(f(\mathbf{p}))$.

parallel distribution defined by

$$f_{\parallel}(p_{\parallel}) = 2\pi \int_0^{\infty} f(p_{\perp}, p_{\parallel}) p_{\perp}\, dp_{\perp}. \quad (4)$$

Finally, the energetic electron population for the range 50 keV $\leq E \leq$ 230 keV is calculated to be $\bar{n}_T \approx 10^{17}$ m^{-3}. The fraction $\bar{n}_T/\bar{n}_e \approx 10^{-3}$ is consistent with other estimates.[12]

In summary, we have successfully deduced an electron-velocity distribution in the energy range 50–230 keV using a much more detailed method of analysis than previously carried out on nonthermal ECE spectra. The nonthermal electron distribution during lower-hybrid heating discharge at $\bar{n}_e = 0.7 \times 10^{20}$ m^{-3} in Alcator C is given as an example. Noteworthy features of the deduced distribution include enhancement in the parallel direction, effective temperature of the energetic distribution of approximately 80 keV, $T_{\perp} \approx 30$ keV, and $T_{\parallel} \approx 200$ keV. This 30-keV $T_{\perp}$ is in rough agreement with that deduced from the first-harmonic intensity. The estimate of the energetic electron-population density is $10^{-3}\bar{n}_e$ in the range 50–230 keV.

We thank all the other members of the Alcator group for their support, especially the radio frequency section, Dr. Porkolab, Dr. Knowlton, Dr. Takase, and Dr. Texter. This work was supported by U.S. Department of Energy under Contract No. DOE-AC02-78ET51013.

[1]D. A. Boyd, in Proceedings of the Fourth International Workshop in Electron-Cyclotron Emission and Electron-Cyclotron-Resonance Heating, Rome, 28–30 March 1984 (unpublished), p. 145.

[2]E. Mazzucato, P. Efthimion, and I. Fidone, Nucl. Fusion **25**, 1681 (1985).

[3]I. H. Hutchinson and K. Kato, Massachusetts Institute of Technology Report No. PFC/JA-85-15, 1985 [Nucl. Fusion (to be published)].

[4]H. P. Freund and C. S. Wu, Phys. Fluids **20**, 963 (1977).

[5]K. Kato and I. H. Hutchinson, Massachusetts Institute of Technology Report No. PFC/RR-84-11, 1984 (unpublished).

[6]K. Kato and I. H. Hutchinson, in Proceedings of the IEEE International Conference on Plasma Science, Pittsburgh, Pa., 3–5 June 1985, IEEE Cat. No. 85CH2199-8, 1985 (unpublished).

[7]M. F. Kimmit, *Far Infrared Techniques* (Methuen, New York, 1970).

[8]K. Swartz, I. H. Hutchinson, and K. Molvig, Phys. Fluids **24**, 1689 (1981).

[9]S. von Goeler *et al.*, Nucl. Fusion **25**, 1515 (1985); S. Texter *et al.*, Bull Am. Phys. Soc. **39**, 1494 (1985).

[10]C. F. F. Karney and N. J. Fisch, Phys. Fluids **22**, 1817 (1979).

[11]D. Hewett *et al.*, in Proceedings of the IAEA Technical Committee Meeting on Non-Inductive Current Drive in Tokamaks, Culham, 18–21 April 1983, Culham Report No. CLM-CD, 1983 (unpublished), Vol. I, p. 124.

[12]M. Porkolab *et al.*, Phys. Rev. Lett. **53**, 1229 (1984).